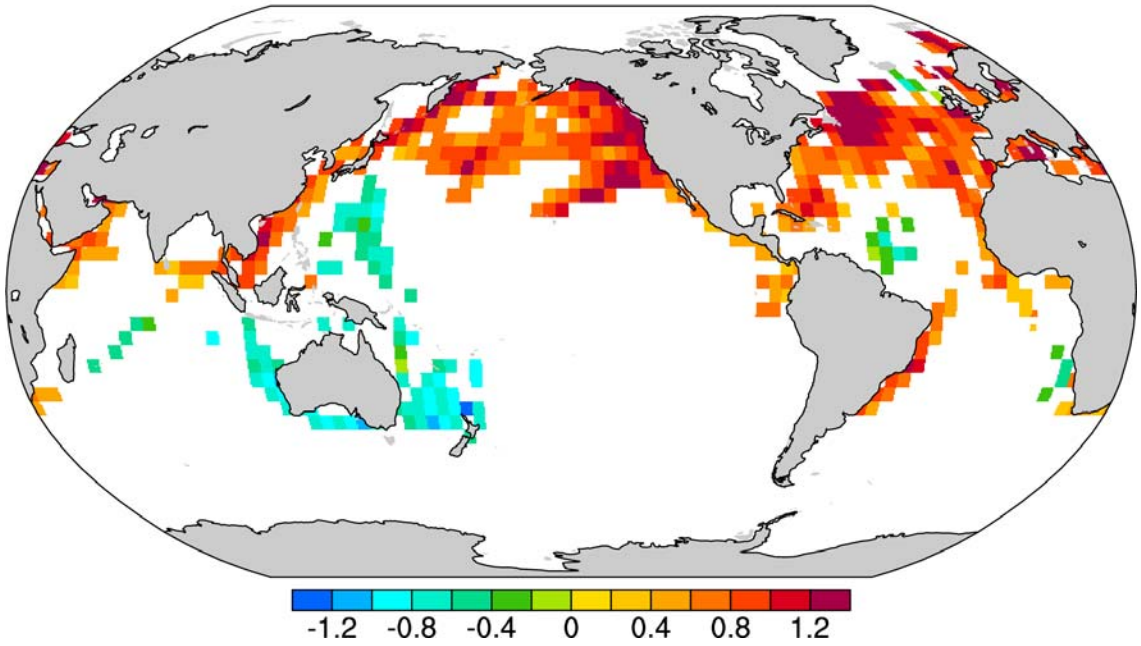

Figure 3.5.3. Estimates of linear trends in significant wave height (cm decade^{-1}) for the regions along the major ship routes for the global ocean for the period 1950–2002. Trends are shown only for the locations where they are significant at the 95% level. Adapted from Gulev and Grigorieva (2004).

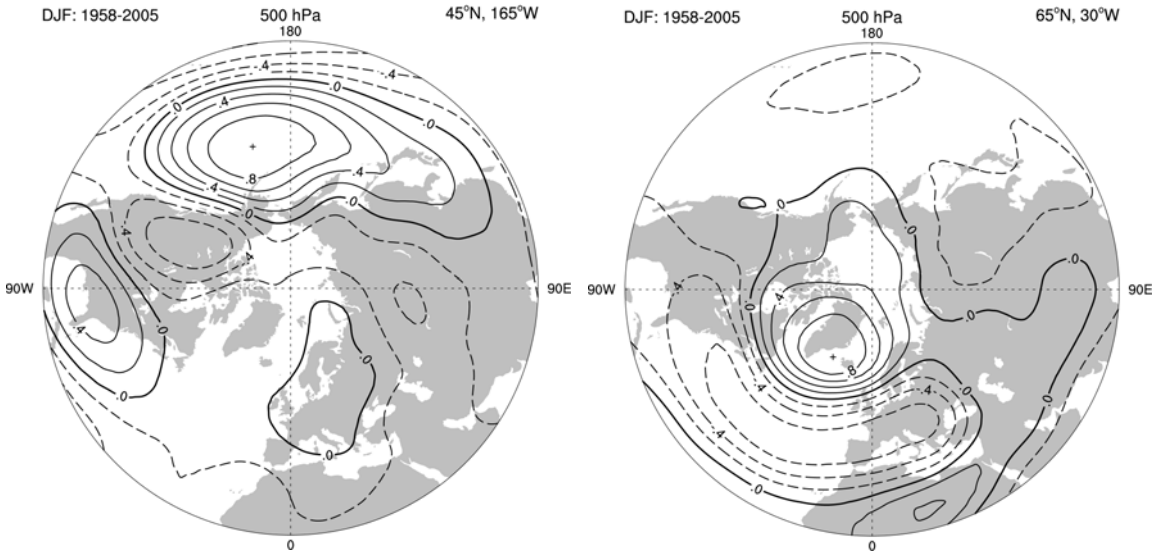

Figure 3.6.1. The PNA (left) and NAO (right) teleconnection patterns, shown as one-point correlation maps of 500 hPa geopotential heights for boreal winter (December–February) over 1958–2005. In the left panel, the reference point is 45ºN, 165ºW, corresponding to the primary centre of action of the PNA pattern, given by the + sign. In the right panel, the NAO pattern is illustrated based on a reference point of 65ºN, 30ºW. Negative correlation coefficients are dashed, and the contour increment is 0.2. Updated from Hurrell et al. (2003).

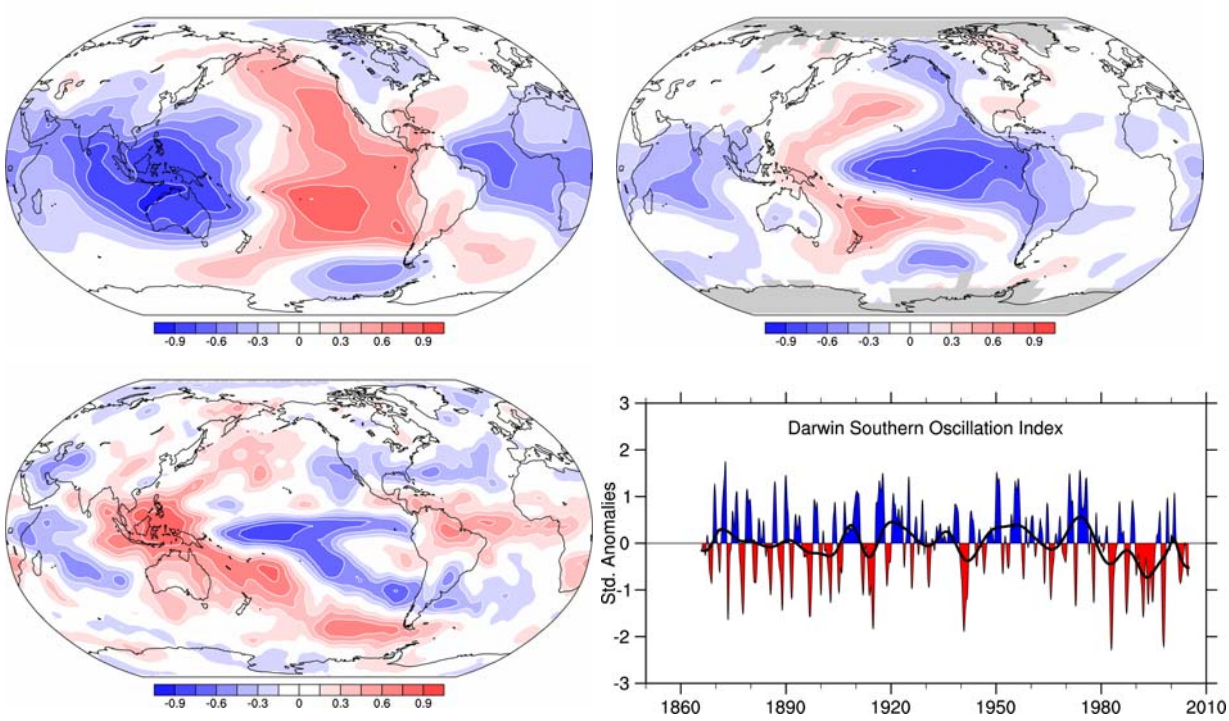

Figure 3.6.2. Correlations with the SO index (SOI) (based on normalised Tahiti minus Darwin sea level pressures) for annual (May to April) means for sea level pressure (top left) and surface temperature (top right) for 1958–2004, and GPCP precipitation for 1979–2003 (bottom left) updated from Trenberth and Caron (2000). The Darwin-based SOI from 1866–2004 (Können et al 1998) (lower right) features seasonal values with an 11-point low frequency filter, which effectively removes fluctuations with periods of less than 8 months (Trenberth, 1984). The heavy line represents a low pass filter (heavy line) to emphasize decadal variability. Red values indicate positive sea level pressure anomalies at Darwin and thus El Niño conditions.

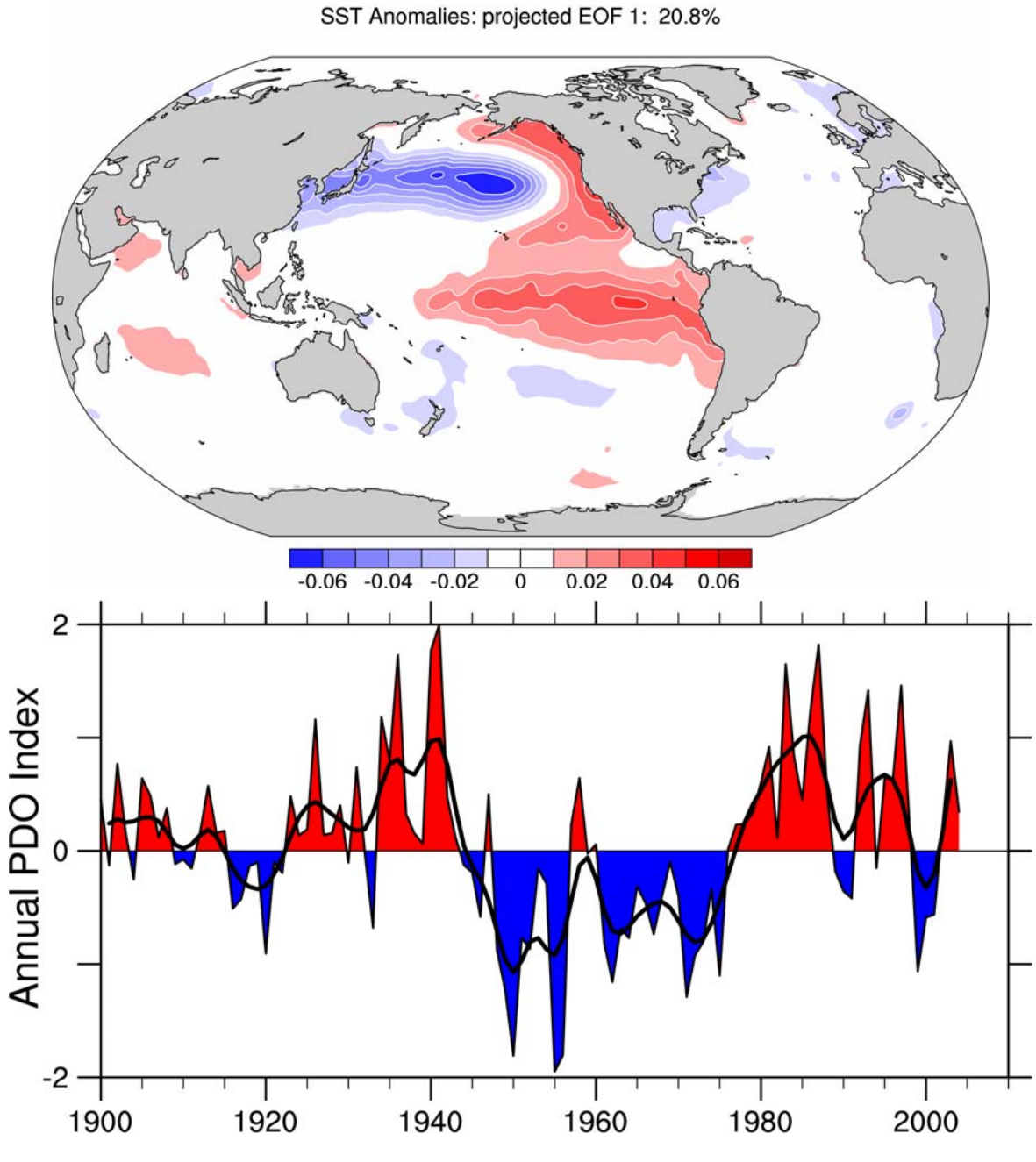

Figure 3.6.3. (a) Sea surface temperature pattern of the Pacific Decadal Oscillation, based on the first EOF SST pattern for the Pacific basin north of 20°N for 1911 to 2004 (updated; see Mantua et al., 1997; Power et al., 1999b) and projected for the global ocean (unitless); and (b) annual time series of the Pacific Decadal Oscillation (updated from Mantua et al., 1997); the low pass filtered heavy curve uses a weighted 7 term 1/24 (1–3–5–6–5–3–1) filter that has a half power point at 11 years to emphasize decadal variations.

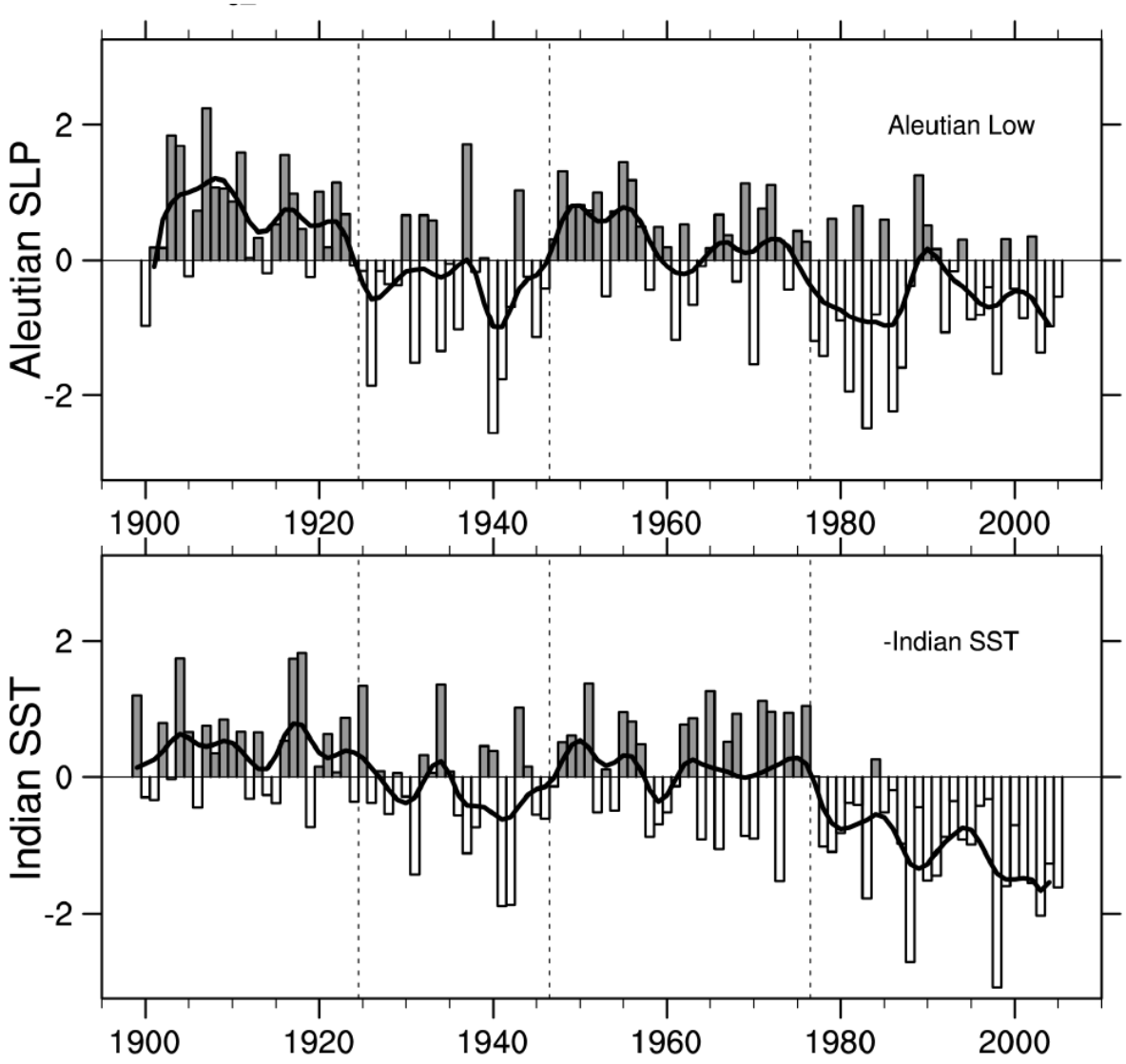

Figure 3.6.4. Top: Time series of the NPI (sea level pressure during December–March averaged over the North Pacific 30º–65ºN, 160ºE–140ºW) from 1900 to 2005 expressed as normalized departures from the long-term mean (each tick mark on the ordinate represents two standard deviations, or 2.8 hPa). This record reflects the strength of the wintertime Aleutian Low Pressure System, with positive (negative) values indicative of a weak (deep) Aleutian Low. The bars give the wintertime series and the thick curve is a low-pass filtered version as in Figure 3.6.3. Values were updated and extended to earlier decades from Trenberth and Hurrell (1994). Lower: As above but for SSTs averaged over the Tropical Indian Ocean (10ºS–20ºN, 50º–125ºE; one standard deviation equals 0.18 K). This record has been inverted to facilitate comparison with (a). The dashed vertical lines mark years of transition in the Aleutian Low record (1925, 1947, 1977). Updated from Deser et al. (2004).

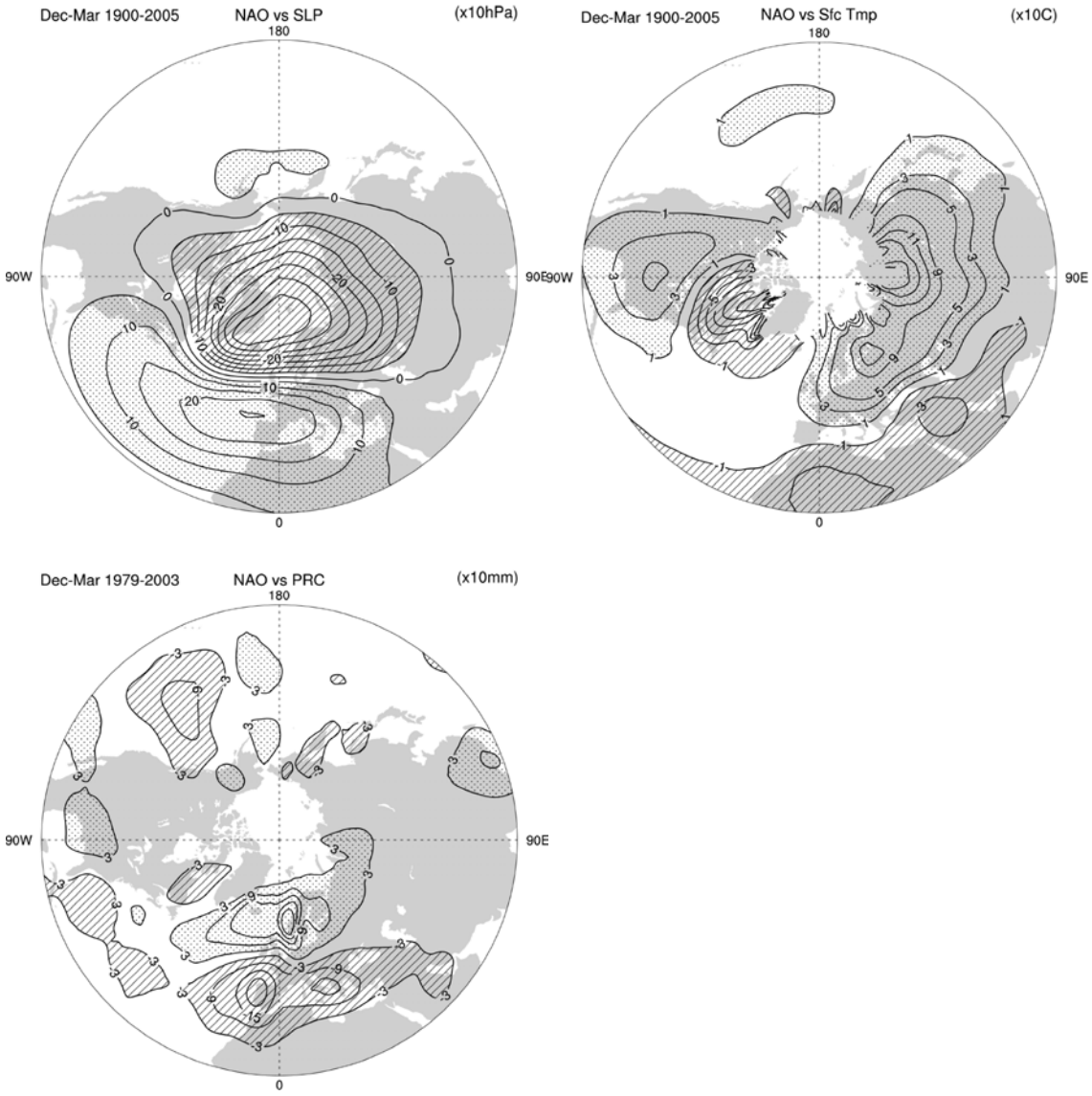

Figure 3.6.5. Changes in mean winter (December–March) corresponding to a unit deviation of the NAO index over 1900–2005 for (top left) sea level pressure in ($\times 10^{-1}$ hPa). Values greater than 0.5 hPa are stippled and <–0.5 hPa are hatched. (Top right) land surface and sea surface temperatures ($\times 10^{-1}$ºC). The contour increment is 0.2ºC. Temperature changes >0.1ºC are indicated by stippling, and those <–0.1 ºC are indicated by hatching. Regions of insufficient data (e.g., over much of the Arctic) are not contoured. (Bottom left) Precipitation for 1979–2003 based on GPCP ($\times 10^{-1}$ mm). Stippling indicates values > 0.3 mm and hatching values less than –0.3 mm/day. Contour interval 0.6 mm/day. Updated from Hurrell et al. (2003).

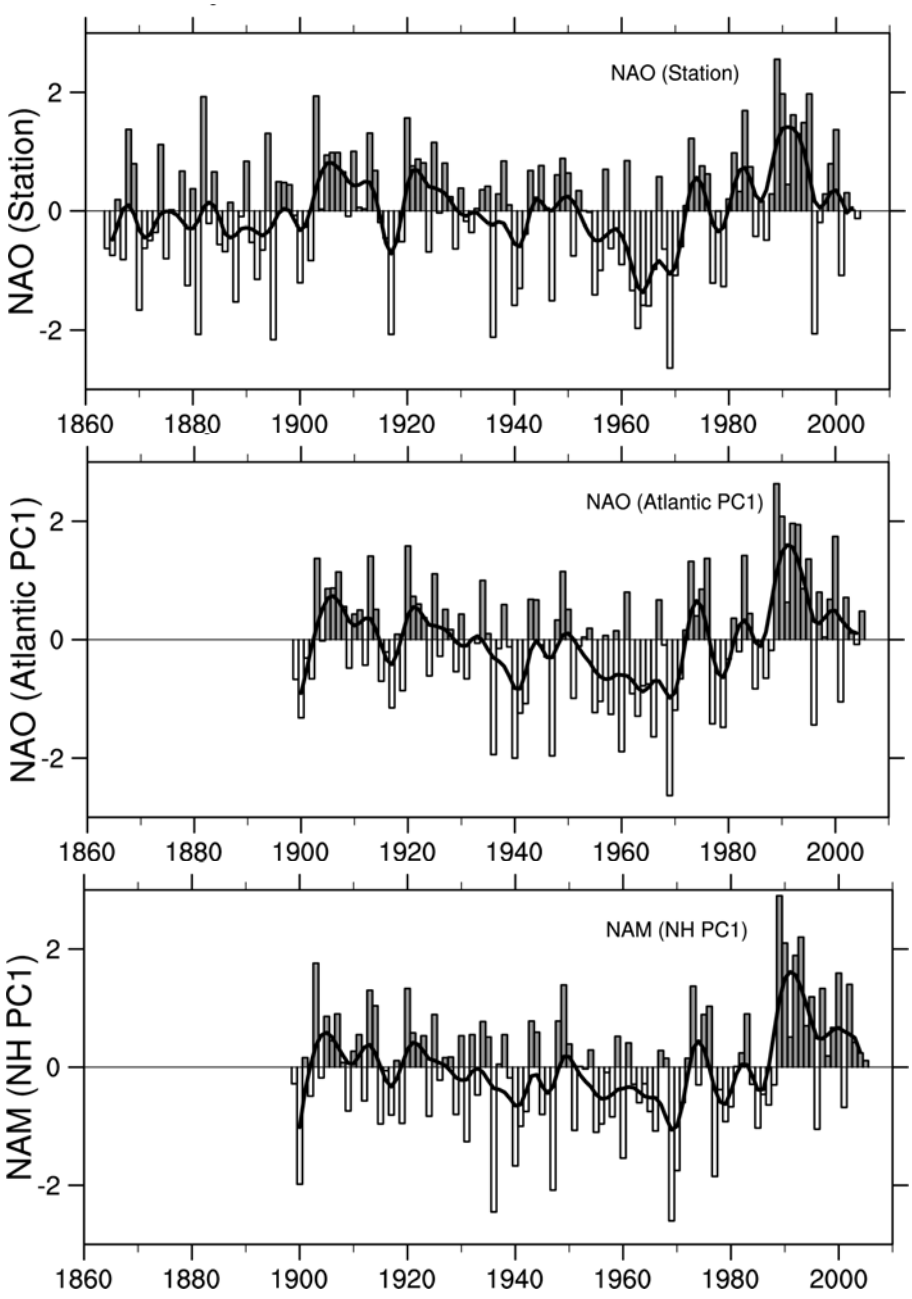

Figure 3.6.6. Normalized indices of the mean winter (December–March) NAO constructed from sea level pressure data. In the top panel, the index is based on the difference of normalized sea level pressure between Lisbon, Portugal and Stykkisholmur/Reykjavik, Iceland from 1864 through 2005. The average winter sea level pressure data at each station were normalized by division of each seasonal pressure by the long-term mean (1864–1983) standard deviation. In the middle panel, the index is the principal component time series of the leading empirical orthogonal function (EOF) of Atlantic-sector sea level pressure. In the lower panel, the index is the principal component time series of the leading EOF of Northern Hemisphere sea level pressure. The heavy solid lines represent the indices smoothed as in Fig. 3.6.3 to emphasize decadal variations. The indicated year corresponds to the January of the winter season (e.g., 1990 is the winter of 1989/1990). See http://www.cgd.ucar.edu/~jhurrell/nao.html for updated time series. Updated from Hurrell et al. (2003).

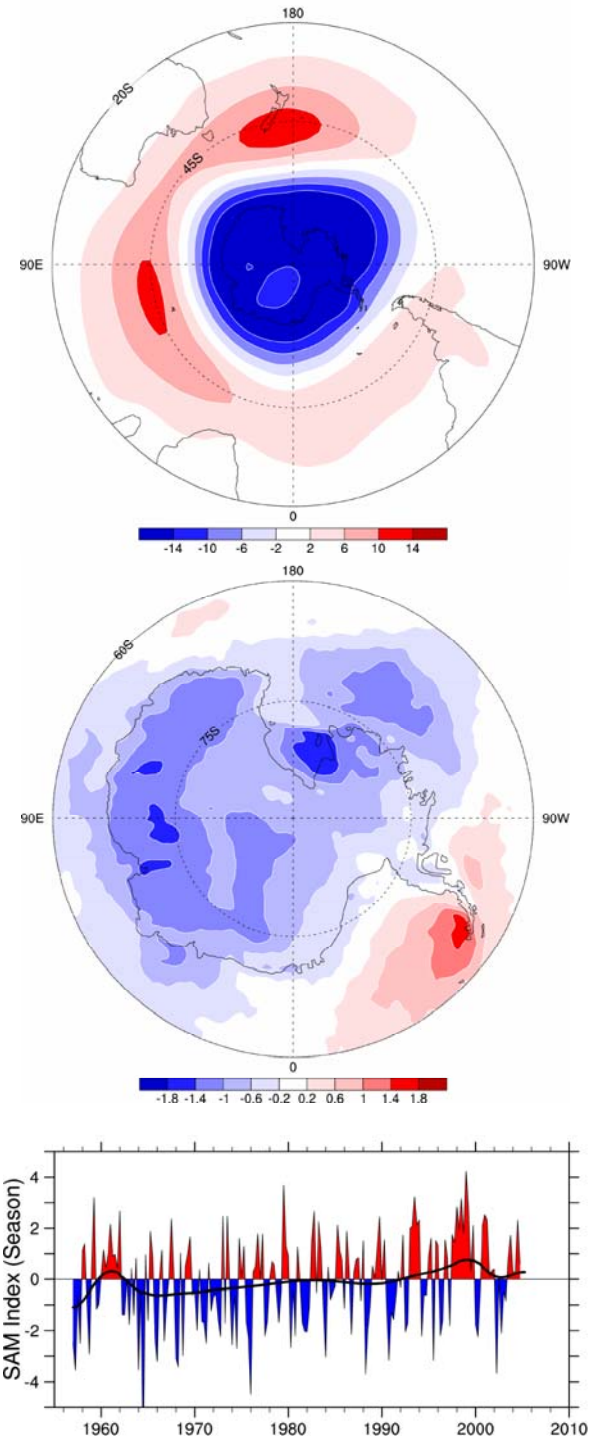

Figure 3.6.7. Bottom: Seasonal values of the SAM index calculated from station data (updated from Marshall, 2003). The low pass filter is the same as in Figure 3.6.3 to emphasize decadal variability. Top: SAM (AAO) geopotential height pattern as a regression based on the SAM time series for seasonal anomalies at 850 hPa (see also Thompson and Wallace, 2000). Middle: the regression of changes in surface temperature over the 23-year period (1982–2004) corresponding to a unit change in the SAM index plotted south of 60ºS. Values exceeding about 0.4°C in magnitude are significant at the 99% confidence levels (updated from Kwok and Comiso, 2002b).

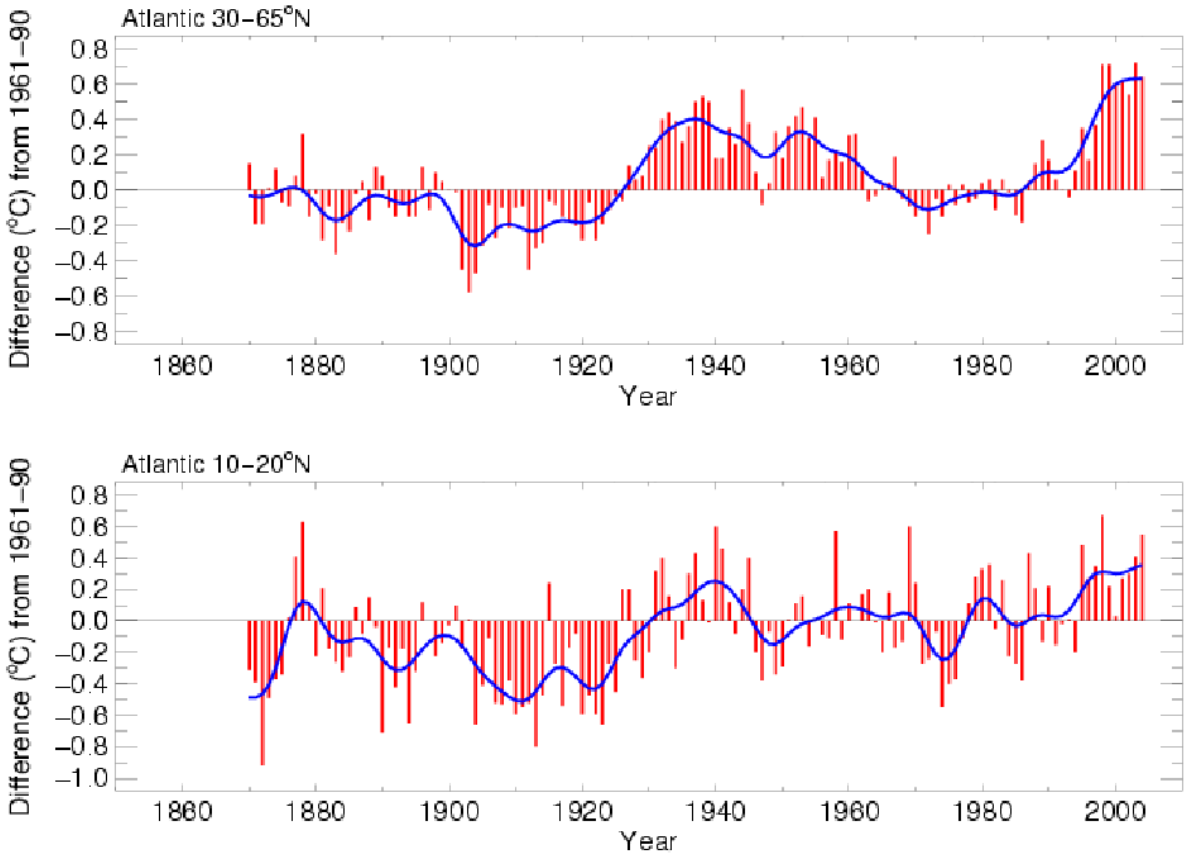

Figure 3.6.8: Atlantic Multidecadal Oscillation index represented by annual anomalies of SST in the extratropical North Atlantic (30–65°N), 1870–2004 (top), and in a more muted fashion in the tropical Atlantic (10–20°N) SST anomalies. Both are relative to 1961 to 1990 mean (°C), after Rayner et al. (2005). The thin bars depict annual means and the smooth curve is after application of a 21-point binomial filter.

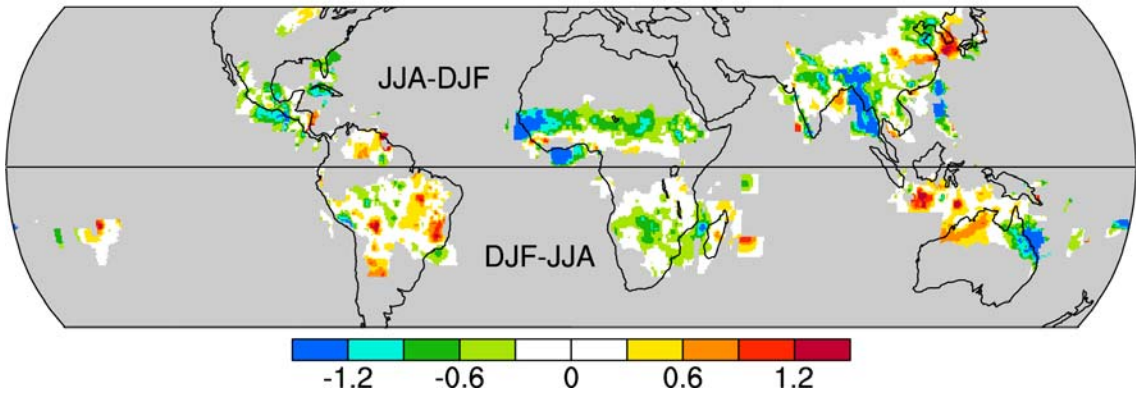

Figure 3.7.1. Change in the epoch mean annual range of precipitation: post-1976 epoch minus pre-1975 epoch in mm/day. Blue/green (red) colour denotes decreasing (increasing) annual rage of the monsoon rainfall. Grey areas indicate missing values. Data used are obtained from NCEP (PREC/L) (Updated from Chen et al., 2004).

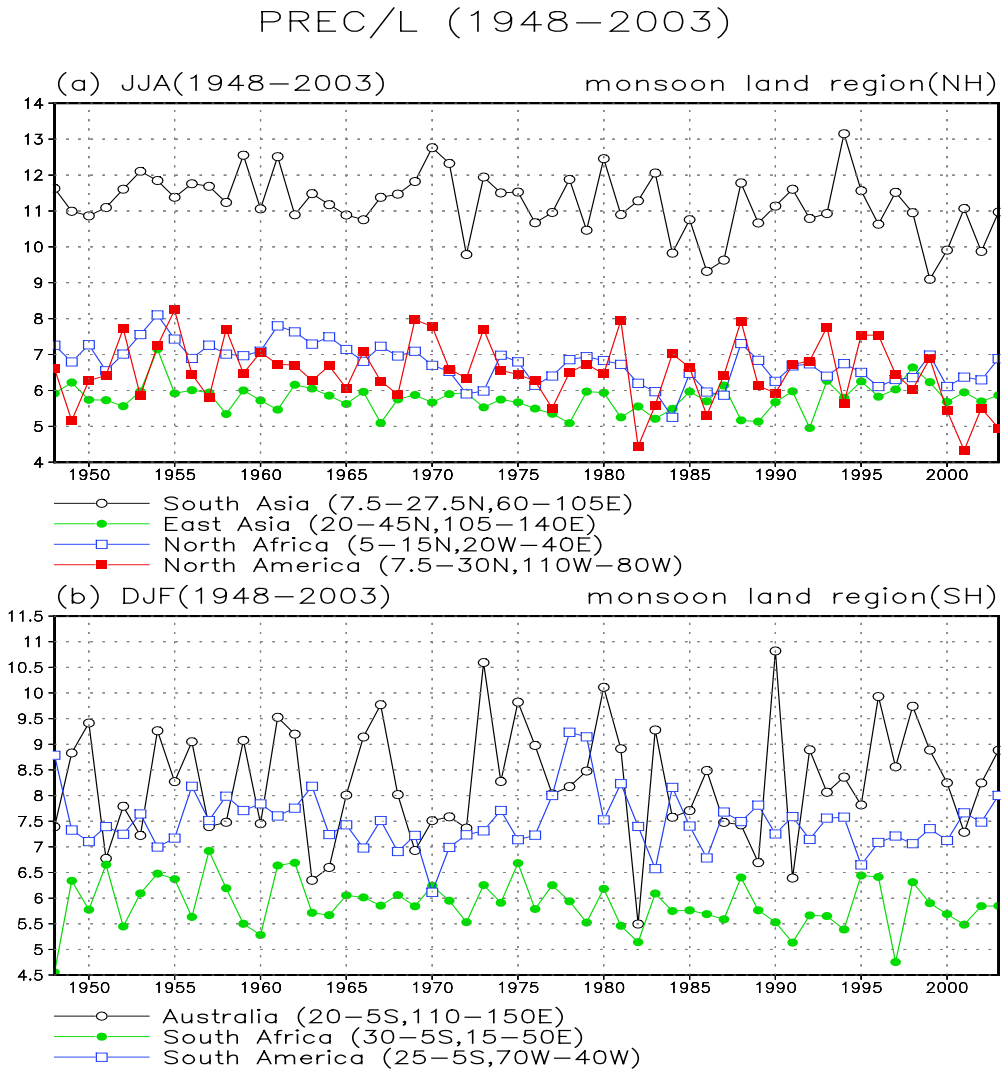

Figure 3.7.2. Time series of the summer mean rainfall rate in each of the monsoon region (land-based observation only) for major NH (a) and SH (b) summer monsoon rainfall regions. Data used are obtained from NCEP (PREC/L) (Chen et al., 2004). To be redone.

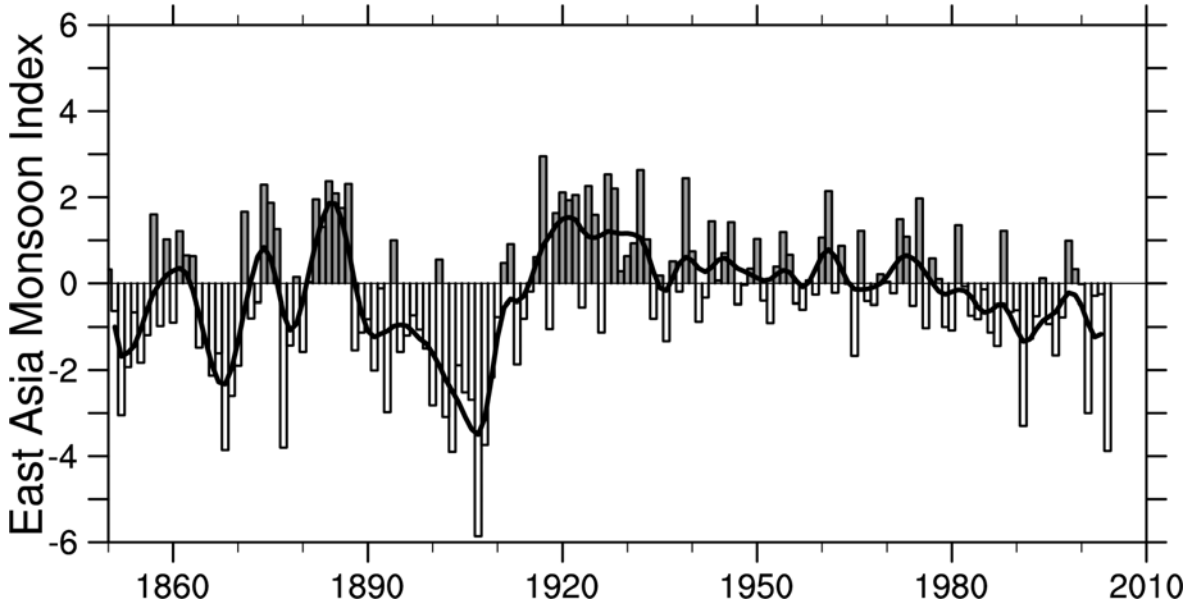

Fig 3.7.3. East Asia summer monsoon index derived from MSLP gradients between land and ocean in the east Asia region. The definition of the index is based on Guo et al. (2003) but was recalculated based on the HadSLP2 data set. Annual values are shown and the black smooth curve is the decadal filter as in Figure 3.6.3.

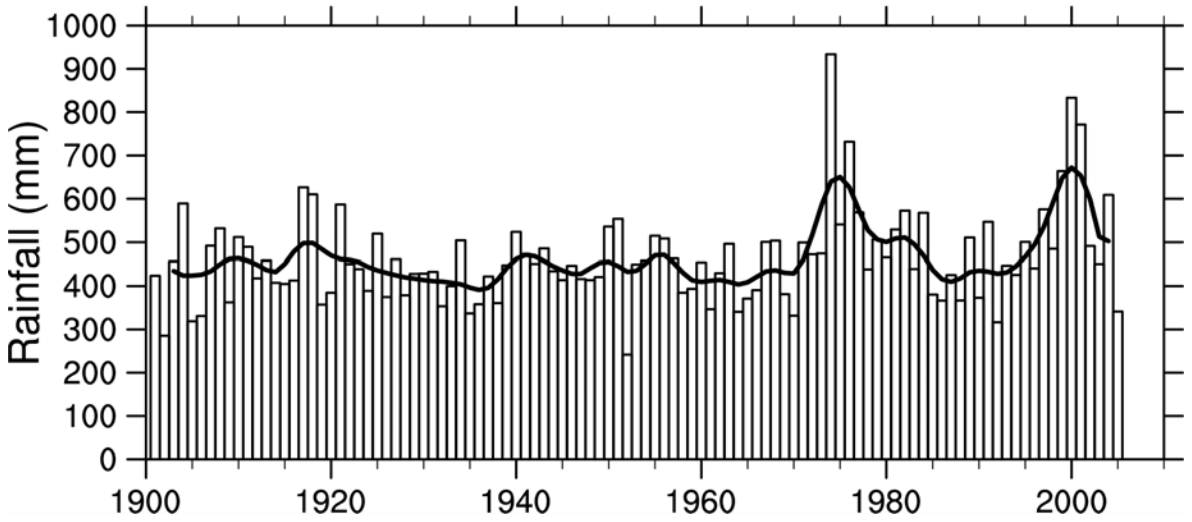

Figure 3.7.4. Times series of northern Australian (north of 26ºS) wet-season (October–April) rainfall during 1900/1901 to 2003/2004. Black curve indicates a low pass filter to illustrate decadal variations, as for Figure 3.6.3. Data from Australian Bureau of Meteorology.

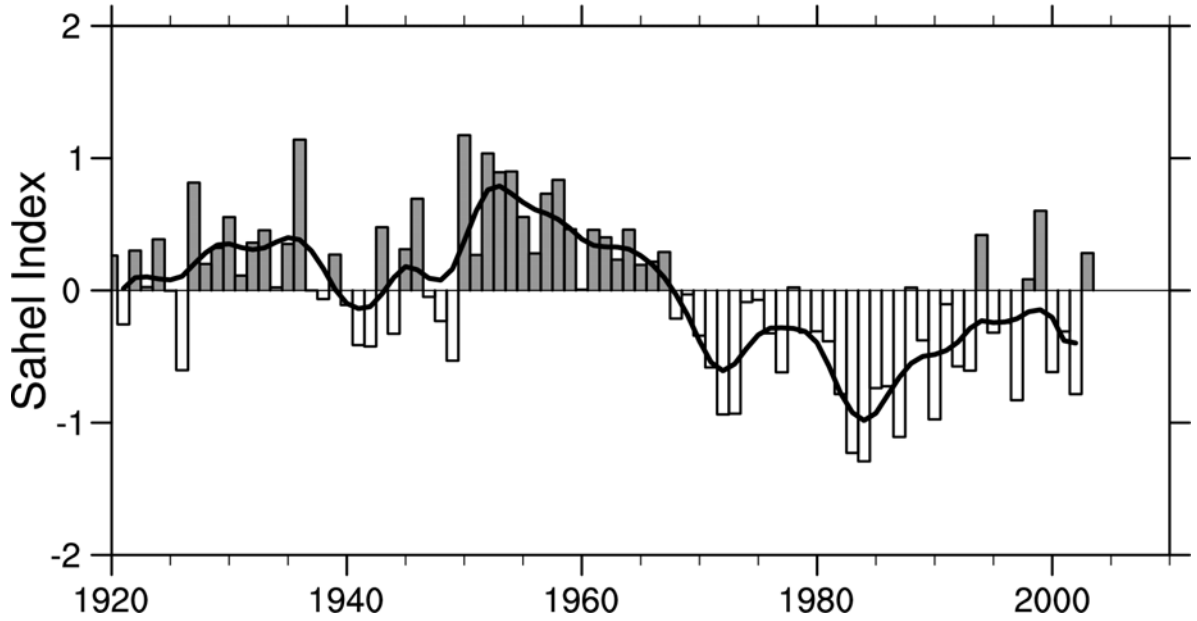

Figure 3.7.5. Time series of Sahel regional rainfall for April–October from 1920 to 2003 derived from gridding normalized station anomalies and then averaging them using area weighting (adapted from Dai et al., 2004a). The low pass filtered (see Figure 3.6.3) heavy curve is designed to show decadal variations.

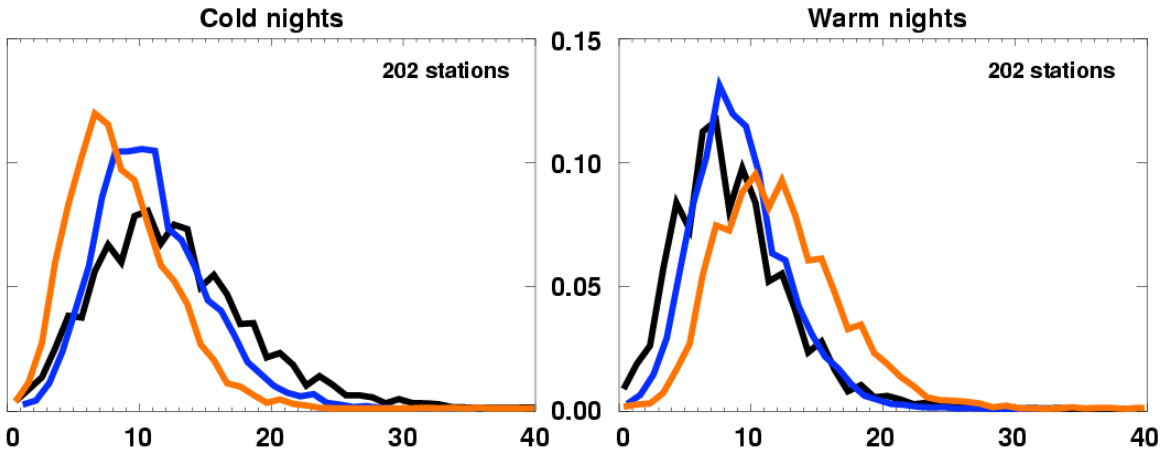

Figure 3.8.1. Annual probability density functions for temperature indices for approximately 200 global stations with at least 80% complete data between 1901 and 2003 for 3 time periods: 1901–1950 (black), 1951–1978 (blue) and 1979–2003 (red). The x-axis represents the percentage of time during the year when the indicators were below the 10th percentile (left) for cold nights or above the 90th percentile (right) for warm nights. From Alexander et al. (2005).

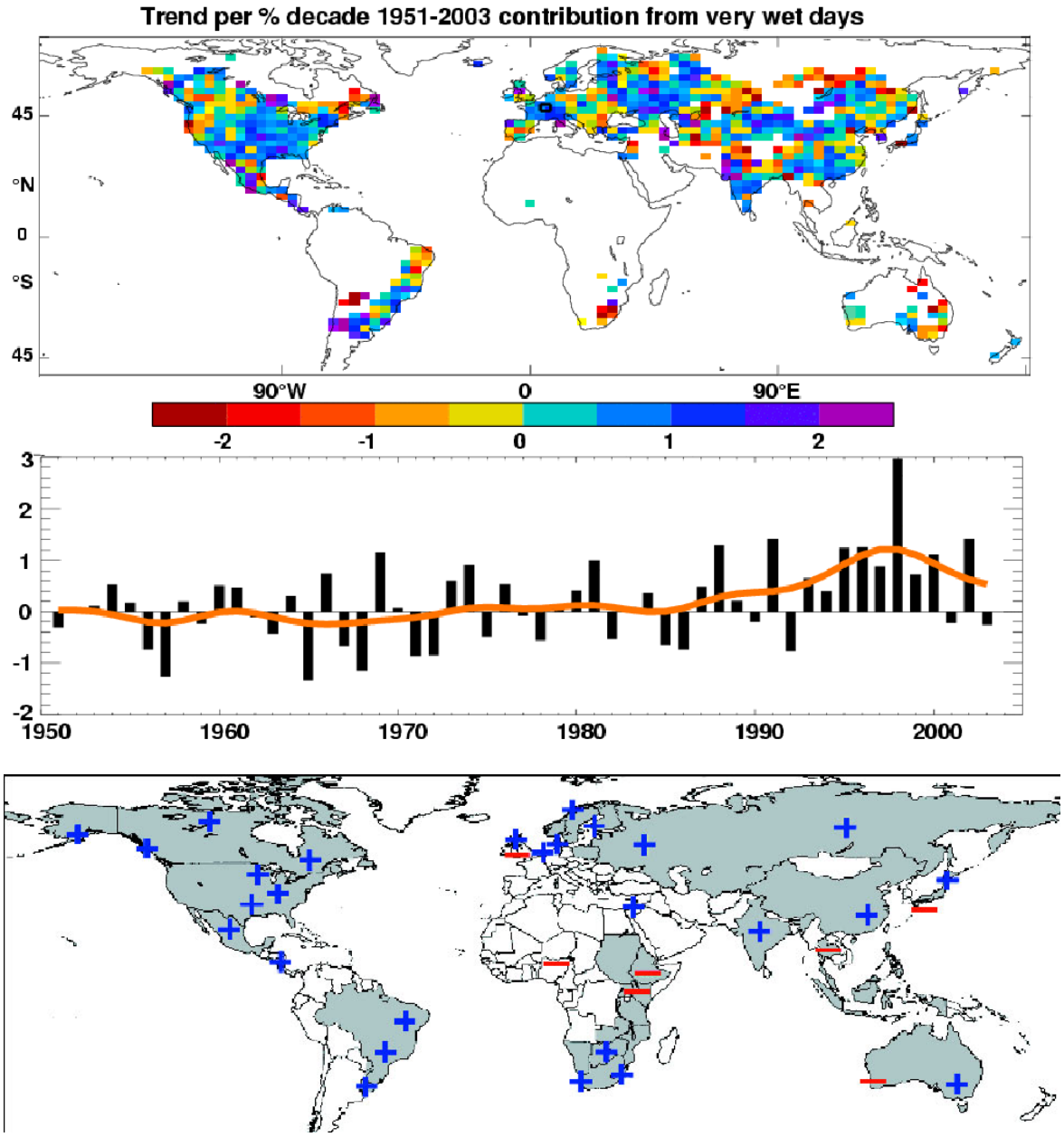

Figure 3.8.2. **a.** Observed trends (%) per decade for 1951–2003 for the contribution to total annual precipitation from very wet days corresponding to the 95th percentile. Trends were only calculated for grid boxes where both total and the 95th percentile had at least 40 years of data during this period and had data until at least 1999. Below the map is the global annual time series anomalies (with respect to 1961–1990) defined as the percentage change from the base period average (22.5%). The red line shows a 21-term binomial fit to the data to show decadal variations. From Alexander et al. (2005). **b.** Regions where disproportionate changes in heavy and very heavy precipitation during the past decades were documented compared to the change in the annual and/or seasonal precipitation updated from Groisman et al. (2005a). Thresholds used to define "heavy" and "very heavy" precipitation vary by season and region. However, changes in heavy precipitation frequencies are always higher than changes in precipitation totals and, in some regions, an increase in heavy and/or very heavy precipitation occurred while no change or even a decrease in precipitation totals was observed.

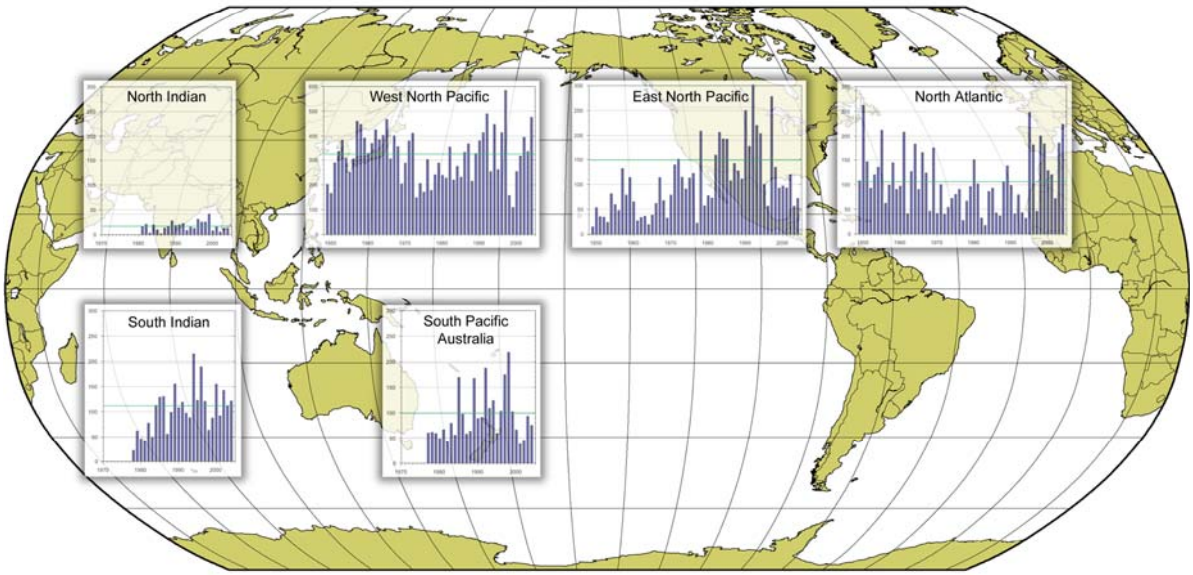

Figure 3.8.3. Seasonal values of the Accumulated Cyclone Energy (ACE) index for the North Indian, South Indian, West North Pacific, East North Pacific, North Atlantic and combined Australian-South Pacific regions. The vertical scale in the West N. Pacific is half that of other basins. The timeline runs from 1948 or 1970 through 2004. The ACE index accounts for the combined strength and duration of tropical storms and hurricanes during a given season by computing the sum of squares of the 6-hour maximum sustained surface winds in knots while the storm is above tropical storm intensity. Based on Levinson (2005).

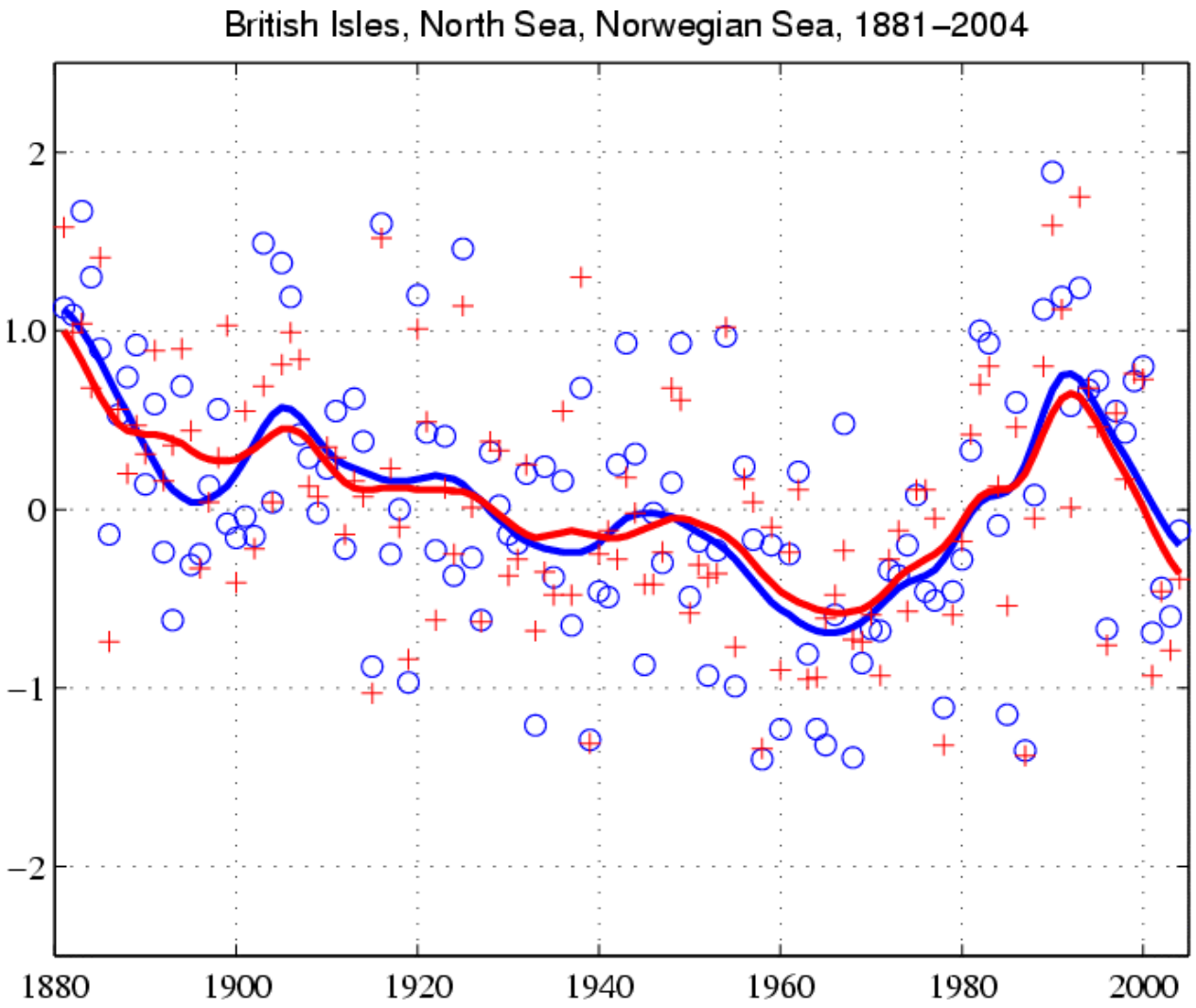

Figure 3.8.4. Storm index for British Isles, North Sea, Norwegian Sea, 1881–2004. Blue circles are 95th percentiles and red crosses 99th percentiles of standardized geostrophic winds averaged over 10 sets of triangles of stations. The smoothed curves are from a Gaussian low pass filter (updated from Alexandersson et al., 2000).

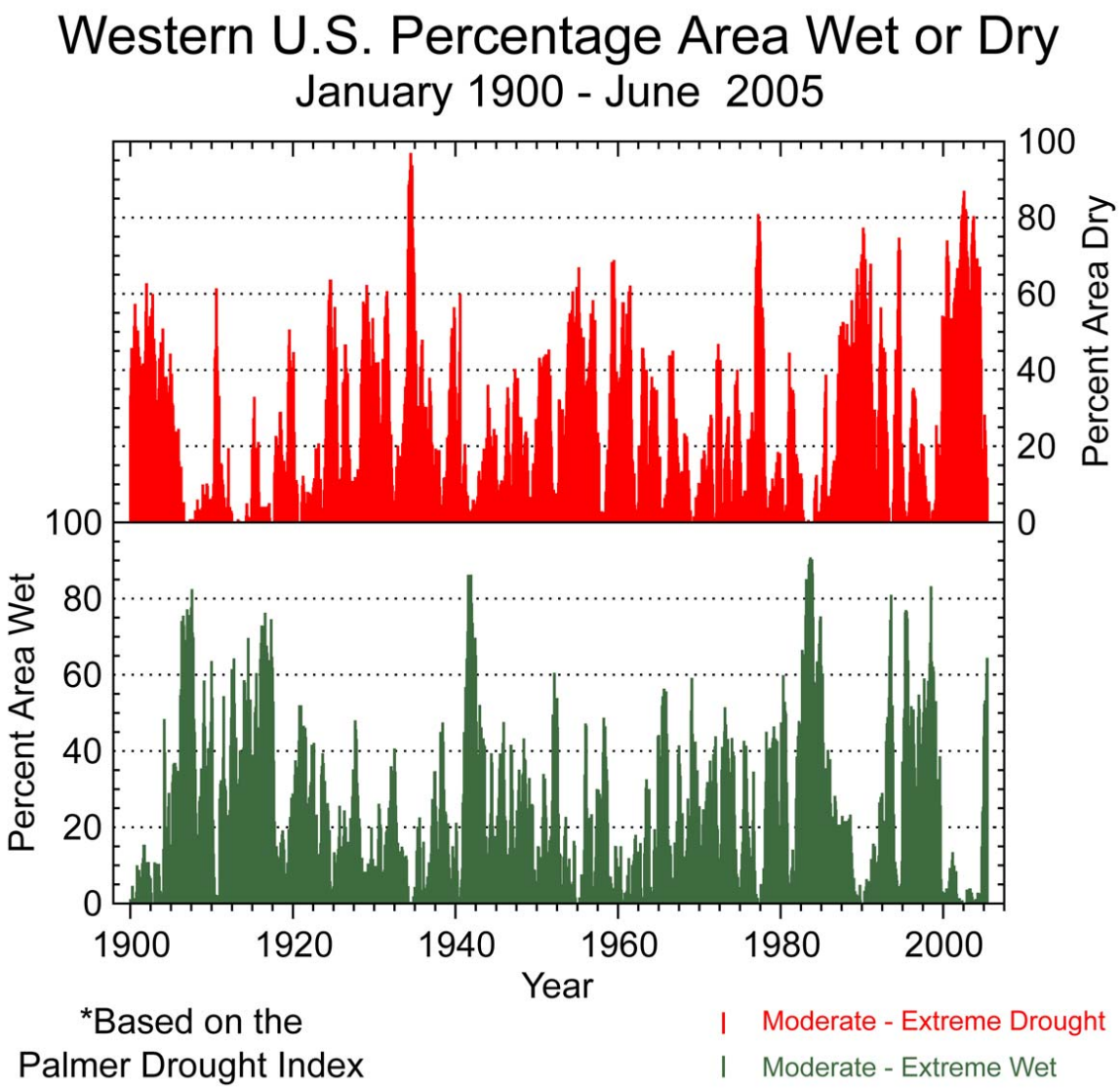

Box 3.5.3, Figure 3.8.5. Percentage of United States west of the Rocky Mountains dry (top) or wet (bottom) based on the Palmer Drought Index for classes moderate to extreme drought or wet. From NOAA NCDC.

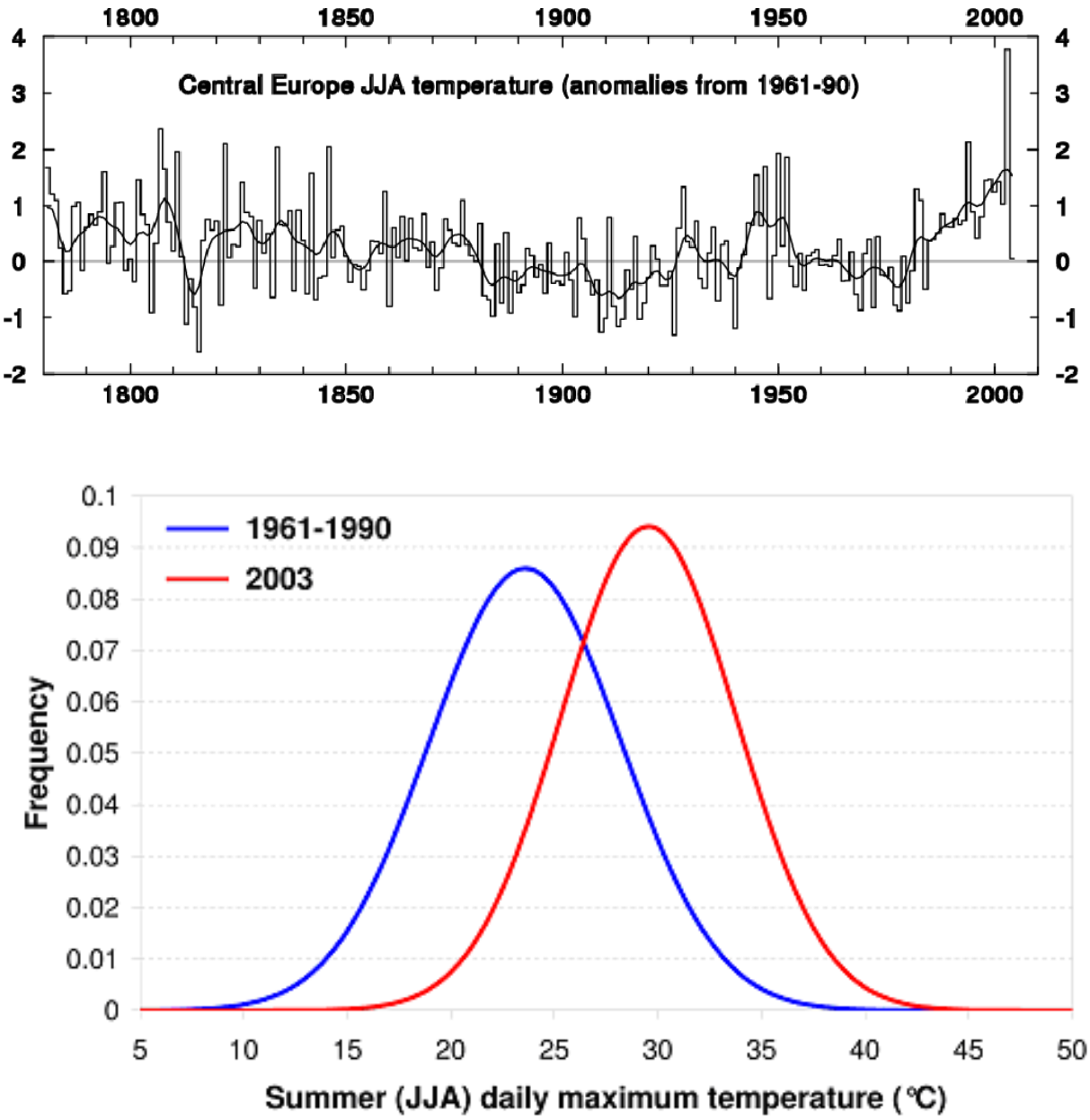

Box 3.6.7, Figure 3.8.6. Long time series of JJA temperature anomalies in Central Europe relative to 1961–1990. In the summer of 2003 values of 3.8°C far exceeded the next largest anomaly of 2.3°C, and the Gaussian distribution (lower panel) of maximum temperatures (red) compared with normal (blue) at Basel, Switzerland shows how the whole distribution was shifted.

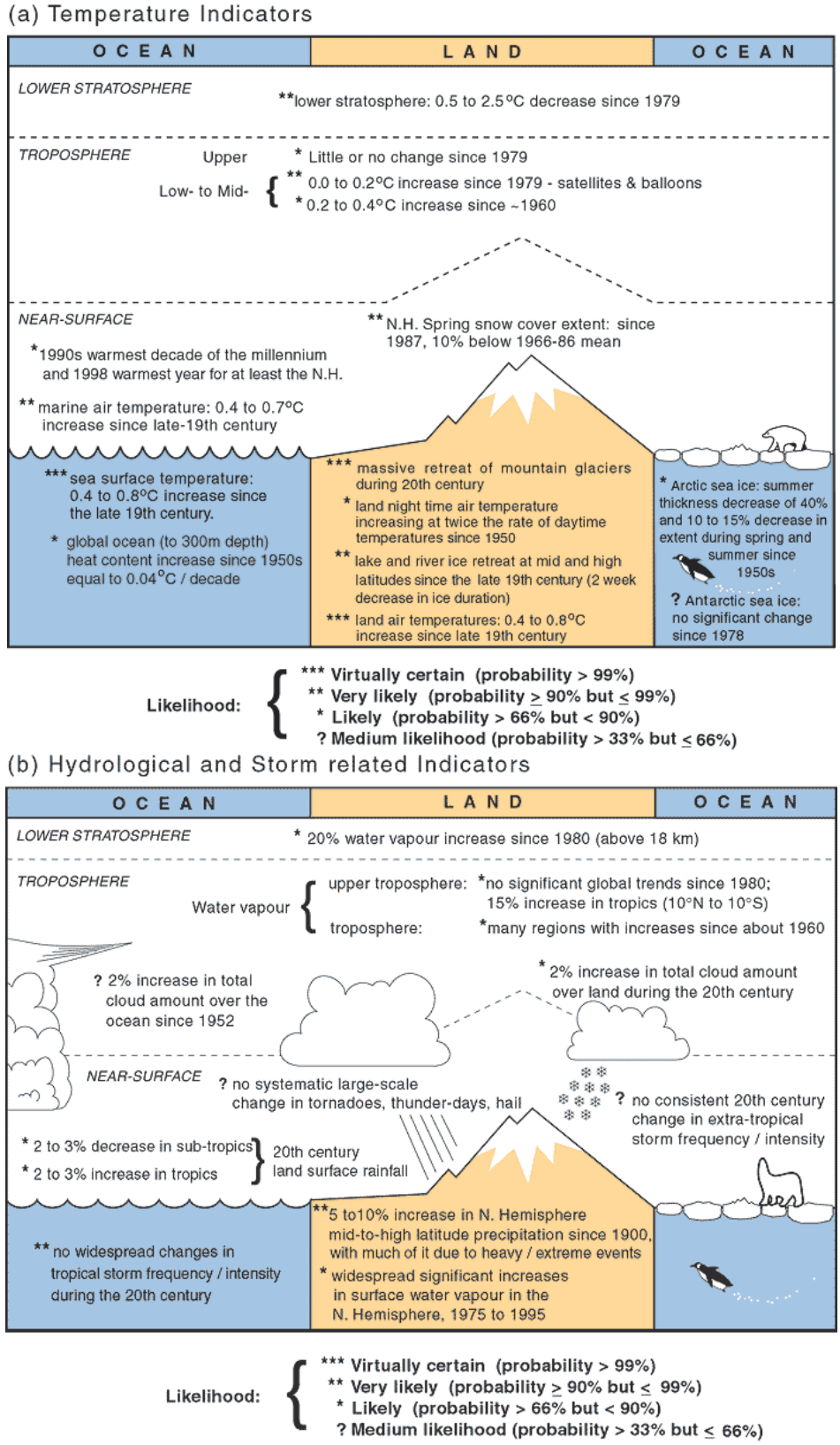

Figure 3.9.1. Currently these are from the TAR.

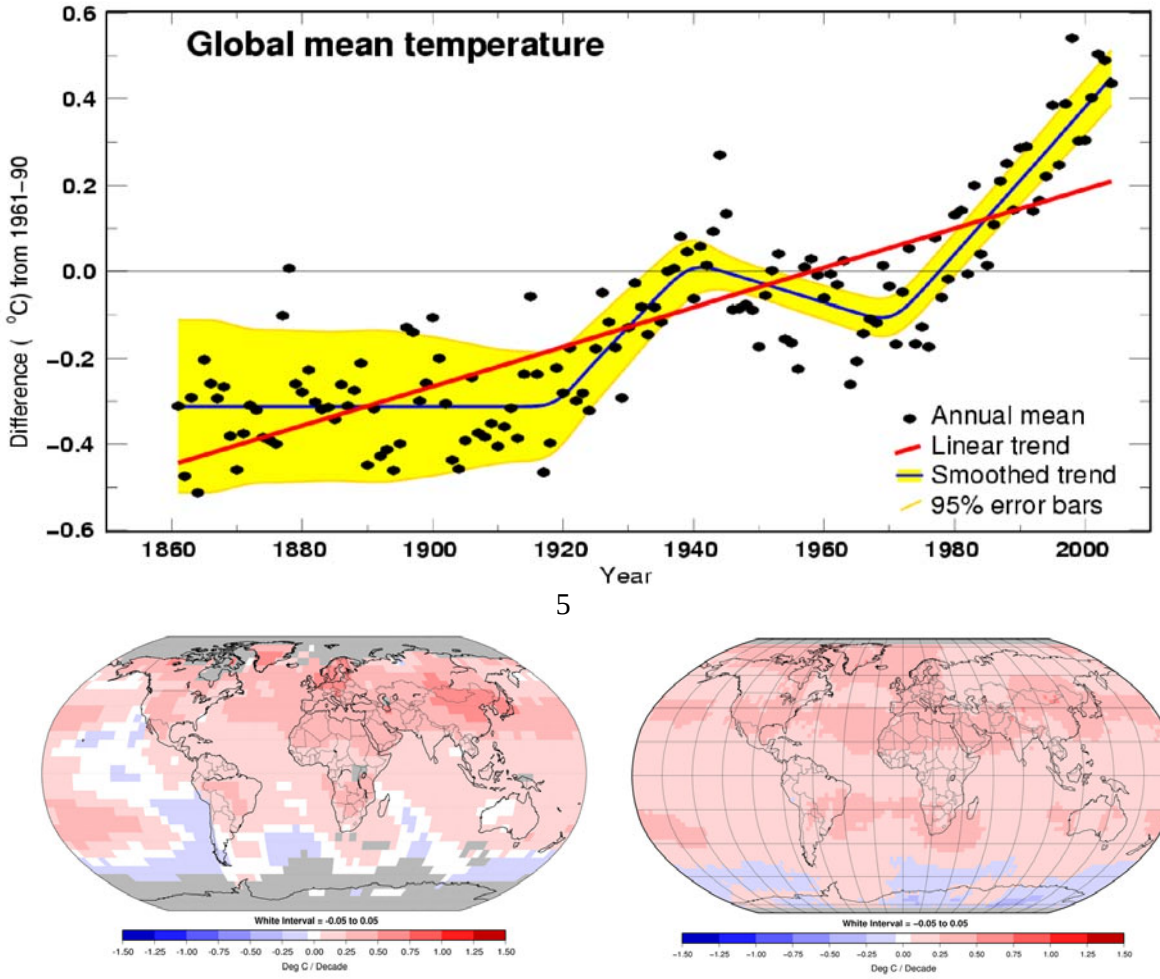

Question 3.1, Figure 1. *Top*: The annual global mean temperatures are given along with simple fits to the data. The red line is a linear trend and the blue line is a smoothed depiction as a series of joining straight line segments with divides at 1920, 1940 and 1970, and with multi-decadal 95% error bars about that line. From model results (Chapter 9), a substantial fraction of the early 20th century warming was contributed by naturally occurring influences including solar radiation changes, volcanism, and natural variability, from 1940 to 1970 the increasing industrialization following World War II increased pollution in the northern hemisphere contributing to cooling, but after the mid-1970s increases in carbon dioxide and other greenhouse gases are believed to dominate the observed warming. *Bottom*: Patterns of linear global temperature trends 1979 to 2004 estimated at the surface, and for the troposphere (from satellite records). Grey areas indicate incomplete data.

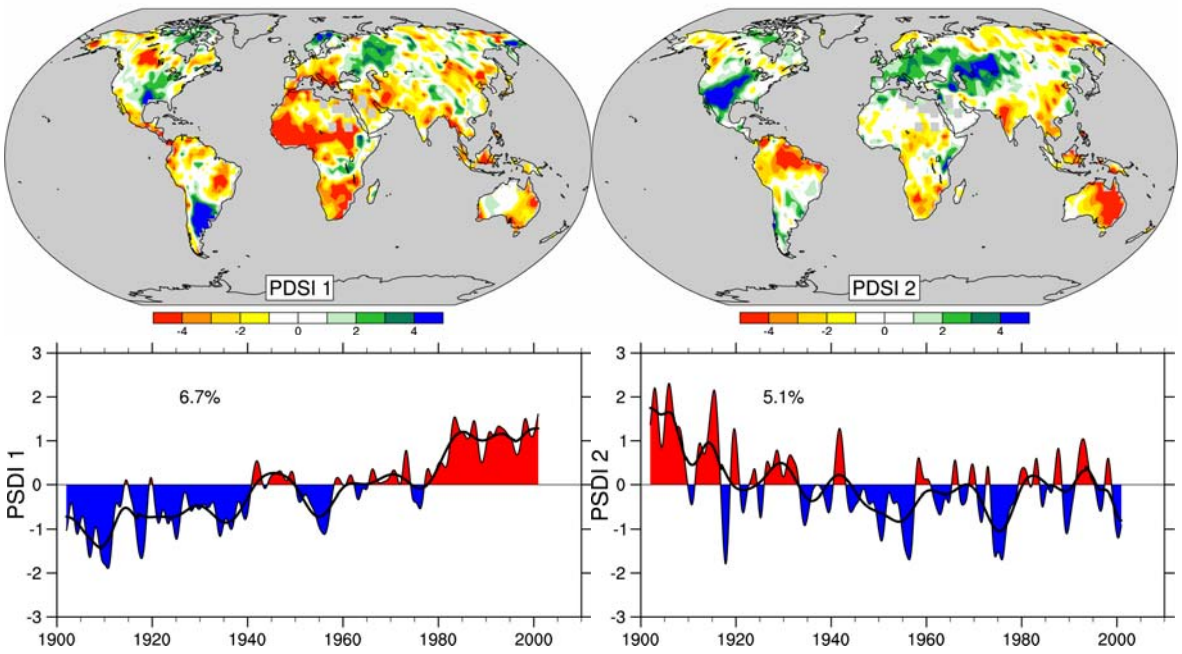

Question 3.2, Figure 1. The two most important spatial patterns (top) of the monthly Palmer Drought Severity Index. The graphs in the lower panels show how the sign and strength of these patterns have changed since 1900. In the top panels, red and orange areas are dryer than average when the values shown in the lower panel graphs are positive. Blue areas in the top panels are wetter when the graphs are positive. The first pattern corresponds to a trend and features the Sahel drought, for instance. The second corresponds very closely to El Niño cycles (except prior to 1915). Adapted from Dai et al. (2004b).

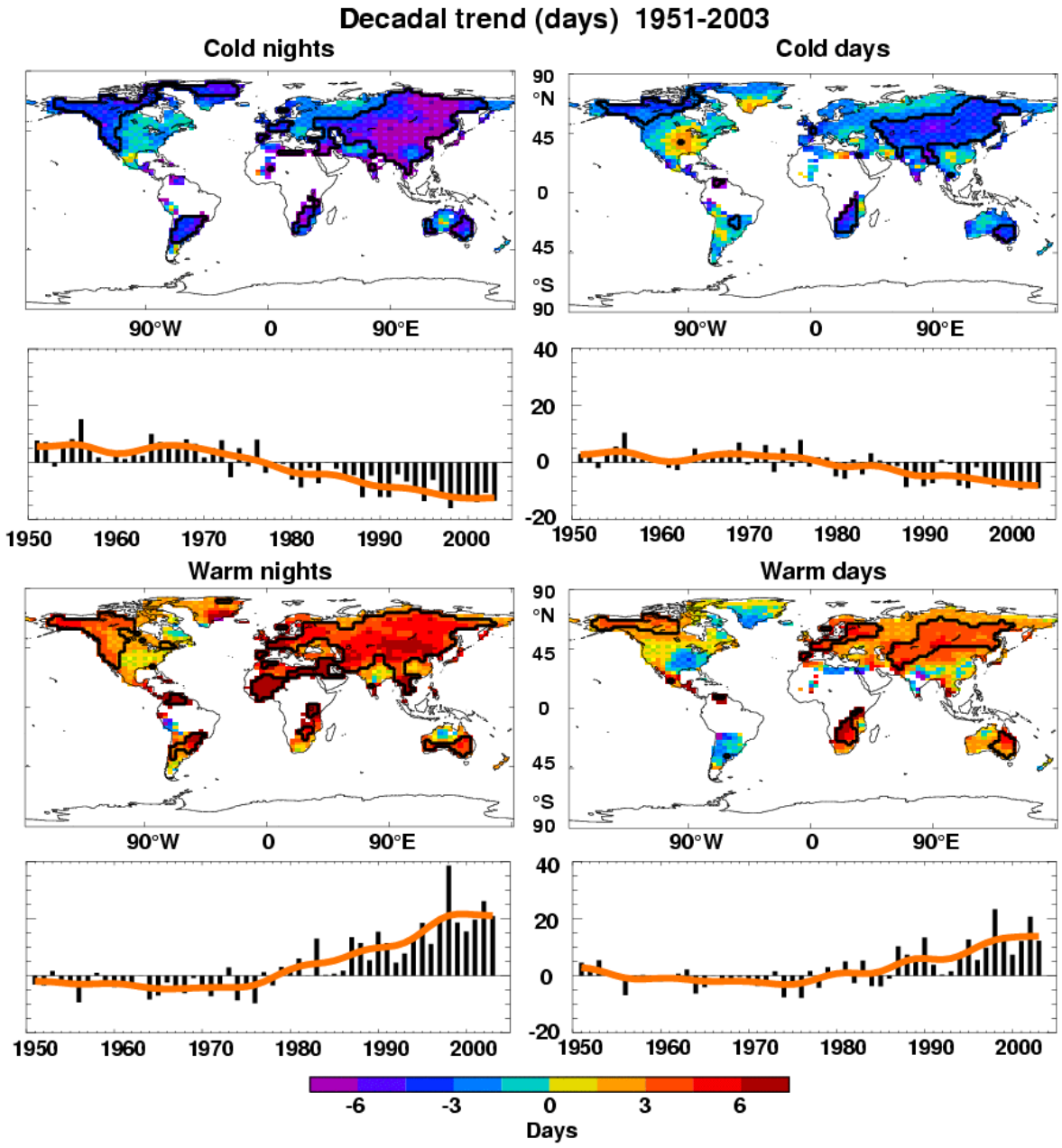

Question 3.3, Figure1. Observed trends (days) per decade for 1951 to 2003 for the percentile temperature indices (a) cold nights, (b) cold days, (c) warm nights, and (d) warm days. Trends were only calculated for grid boxes that had at least 40 years of data during this period and had data until at least 1999. Black lines enclose regions where trends are significant at the 5% level. Below each map is the global annual time series anomalies (with respect to 1961–1990). The red line shows a 21-term binomial fit to the data to show decadal variations. Trends are significant at the 5% level for all the indices shown using a modified Kendall tau test. From Alexander et al. (2005a).